J. Fluid Mech. (1999), *vol.* 379, *pp.* 165–190. Printed in the United Kingdom

Effects of the Lewis number and radiative heat loss on the bifurcation and extinction of CH_4/O_2-N_2-He flames

By YIGUANG JU[1]†, HONGSHENG GUO[2], FENGSHAN LIU[3] AND KAORU MARUTA[4]

[1]Department of Aeronautics and Space Engineering, Tohoku University, Aramaki Aoba, Aoba-ku, Sendai 980, Japan

[2]Centre for Advanced Gas Combustion Technology, Department of Chemical Engineering, Queen's University at Kingston Ontario, K7L 3N6 Canada

[3]Combustion Research Group, Bldg M-9, Institute for Chemical Process and Environmental Technology, National Research Council, Ottawa, K1A 0R6 Canada

[4]Institute of Fluid Science, Tohoku University, Sendai 980-77, Japan

(Received 13 August 1997 and in revised form 27 July 1998)

Effects of the Lewis number and radiative heat loss on flame bifurcations and extinction of CH_4/O_2-N_2-He flames are investigated numerically with detailed chemistry. Attention is paid to the interaction between radiation heat loss and the Lewis number effect. The Planck mean absorption coefficients of CO, CO_2, and H_2O are calculated using the statistical narrow-band model and compared with the data given by Tien. The use of Tien's Planck mean absorption coefficients overpredicts radiative heat loss by nearly 30 % in a counterflow configuration. The new Planck mean absorption coefficients are then used to calculate the extinction limits of the planar propagating flame and the counterflow flame when the Lewis number changes from 0.967 to 1.8. The interaction between radiation heat loss and the Lewis number effect greatly enriches the phenomenon of flame bifurcation. The existence of multiple flames is shown to be a physically intrinsic phenomenon of radiating counterflow flames. Eight kinds of typical patterns of flame bifurcation are identified. The competition between radiation heat loss and the Lewis number effect results in two distinct phenomena, depending on if the Lewis number is greater or less than a critical value. Comparisons between the standard limits of the unstrained flames and the flammability limits of the counterflow flames indicate that the flammability limit of the counterflow flame is lower than the standard limit when the Lewis number is less than the critical value and is equal to the standard limit when the Lewis number is higher than this critical value. Finally, a G-shaped curve and a K-shaped curve which respectively represent the flammable regions of the multiple flames for Lewis numbers lower and higher than the critical value are obtained. The G- and K-shaped curves show a clear relationship between the stretched counterflow flame and the unstrained planar flame. The present results provide a good explanation of the physics revealed experimentally in microgravity.

† Author to whom correspondence should be addressed: e-mail ju@ju.mech.tohoku.ac.jp.

1. Introduction

Thermal radiation is an important, often dominant, heat transfer mechanism in combustion systems. It is well known that radiative heat loss produces a lean and rich concentration limit for one-dimensional unstrained flames (Coward & Jones 1952; Spalding 1957; Buckmaster 1976; Lakashima, Paul & Mukunda 1988; Sibulkin & Frendi 1990; Law & Egolfopoulos 1992). These limits are sometimes called standard limits. For stretched flames, however, although several studies have been conducted to consider the effect of radiation heat loss and upstream heat loss (Sohrab & Law 1984; Tien 1986; Cetegen & Pines 1992; Dixon-Lewis 1994; Egolfopoulos 1994) on the stretch extinction, the radiation-induced extinction at low stretch rate received less attention. To date, the question of how the flammability limit of a stretched flame is related to the standard limit remains unresolved in the combustion literature. On the experimental side, a linear extrapolation method was suggested by Law, Zhu & Yu (1986) to determine the standard limit by extrapolating the stretch extinction limit of counterflow flames to zero stretch rate. Although it predicted reasonable results in some practical applications, this experiment-based method lacks sound theoretical ground. On the other hand, the application of the flamelet concept to turbulent combustion also requires an accurate determination of the flammability limit and the flame regimes of the stretched flame.

Recent development of microgravity experiment provides an ideal environment to observe combustion phenomena near the flammability limit. Studies of radiating flames at low stretch rates were usually conducted using the spherically propagating flame (Ronney 1985, 1988; Lovachev 1990; Sibulkin & Frendi 1990). The experimental studies in microgravity by Ronney (1985, 1988) showed that flames self-extinguish as they expand outward when the fuel concentration is lower than the standard limit.

For counterflow flames, although a number of studies (Sohrab & Law 1984; Liu, Ye & Sohrab 1986) were conducted to investigate the effects of radiation heat loss on extinction, the combined effects of radiation and stretch, particularly at low stretch rate, were not described. In pioneering work, done later, Platt & Tien (1990) found that there is a radiation-induced extinction point at low stretch rate. A recent experiment by Maruta *et al.* (1996) revealed that there are two distinct extinction points at low and high stretch rates respectively for methane/air flames. Numerical studies carried out by Guo *et al.* (1997) and Sung & Law (1996) with detailed chemistry produced a C-shaped extinction curve and showed that the extinction at low stretch rate observed in the experiment is caused by radiation heat loss. However, the above studies have not yet answered the question of how the flammability limit of counterflow flames is related to the standard limit. Further examination by Ju *et al.* (1997*b*) revealed a phenomenon of multiple flame bifurcation and obtained a G-shaped extinction curve. Their results show that the flammability limit of counterflow flames is much lower than the standard limit. Furthermore, the results showed that two kinds of flame, a normal flame and a weak flame, can co-exist at the same stretch rate. Coincidentally, a theoretical study conducted independently by Buckmaster (1997) showed that there are four kinds of flame bifurcations and also indicated that two kinds of stable flames might be sustained at the same stretch rate.

Extinction experiments on a propane/air flame in microgravity (Maruta *et al.* 1995), however, showed an extinction curve distinct from that of a methane/air flame. In addition, extensive experimental and theoretical studies have shown that the Lewis number has a great impact on the stretch extinction (Sivashinsky 1976; Sato 1982; Ishizuka & Law 1982). Therefore, the question of how the G-shaped curve evolves

with the increase of the Lewis number naturally arises. A numerical study by Ju *et al.* (1998) using one-step chemistry and constant transport properties showed that the phenomena of flame bifurcation and flame extinction are greatly enriched by the interaction of radiation heat loss and the Lewis number effect. It was found that a transition from the G-shaped extinction curve to a K-shaped one occurs as the Lewis number increases.

On the other hand, although spectral radiative transfer calculations have been considerably improved in the last decade, the Planck mean absorption coefficients used in the optically thin approximation made in the studies of flame radiation are still those given by Tien (1968). Therefore, there is a crucial need to examine the accuracy of Tien's data.

The objective of this study is to investigate numerically the effects of Lewis number on flame bifurcation and extinction of radiating CH_4/O_2-N_2-He flames using detailed chemistry and transport properties and the new Planck mean absorption coefficients. The Lewis number of the mixture is changed from 0.967 to 1.8 by partly replacing N_2 in air with He. The paper is organized as follows. First, the Planck mean absorption coefficients of CO, CO_2, and H_2O are calculated using the statistical narrow-band model and the discrete ordinates method. The accuracy of the present data and Tien's data is assessed in the calculation of a counterflow flame. Then extinction limits of the planar unstrained CH_4/O_2-N_2-He flames are calculated. This is followed by an examination of flame bifurcations of the corresponding counterflow flames. Several typical kinds of flame bifurcations are then summarized. Finally, the flammability limits of counterflow flames are compared with the corresponding standard limits of planar unstrained flames. Extinction curves for low and high Lewis numbers are obtained.

2. Theoretical models

Two kinds of flame configurations are considered in this study. The first configuration is the one-dimensional planar propagating flame (unstrained flame). The flame propagates towards the unburned side at a speed of S_L in a CH_4/O_2-N_2-He mixture. By attaching the spatial coordinate to the flame front, the governing equations for an isobaric one-dimensional flame can be written as

$$\frac{\partial \dot{m}}{\partial x} = 0, \tag{1}$$

$$\rho C_p \frac{\partial T}{\partial t} + \dot{m} C_p \frac{\partial T}{\partial x} = \frac{\partial}{\partial x}\left(\lambda \frac{\partial T}{\partial x}\right) - \sum_{k=1}^{n} \rho Y_k V_k C_{pk} \frac{\partial T}{\partial x} - \sum_{k=1}^{n} \dot{\omega}_k h_k M_k + \dot{q}_r, \tag{2}$$

$$\rho \frac{\partial Y_k}{\partial t} + \dot{m} \frac{\partial Y_k}{\partial x} = -\frac{\partial}{\partial x}(\rho Y_k V_k) + \dot{\omega}_k M_k, \quad k = 1, n, \tag{3}$$

$$p = \rho \sum_{k=1}^{n} Y_k \frac{R_0}{M_k} T, \tag{4}$$

$$\frac{\partial Y_F}{\partial x} = 0, \tag{5}$$

where x denotes the spatial coordinate perpendicular to the flame front, ρ, p and T are respectively the mass density, pressure and temperature. Y_k, M_k, C_{pk} and V_{kx} are respectively the mass fraction, molecular weight, constant-pressure heat capacity and diffusion velocity in the x-direction of the kth species. Y_F and $\dot{m}$ are the mass fraction

of fuel and the mass flow rate, respectively. R_0 and $\dot{\omega}_k$ are the gas constant and molar production rate of species k. $\dot{q}_r$ is the volumetric radiation heat loss term and will be described in the next section. The upstream boundary conditions can be specified as

$$T = T_{-\infty}, \quad Y_{k\neq F} = Y_{k,-\infty}, \quad \frac{\partial Y_F}{\partial x} = 0, \tag{6}$$

and the downstream boundary conditions are

$$\frac{\partial T}{\partial x} = 0, \quad \frac{\partial Y_{k\neq F}}{\partial x} = 0, \quad \frac{\partial Y_F}{\partial x} = 0. \tag{7}$$

It should be noted here that the upstream boundary must be chosen sufficiently far away from the flame front to make the diffusion flux negligible. In addition, in order to close the above equation systems, two interior boundary conditions are required to specify the mass flux rate $\dot{m}$ and the fuel concentration Y_F. This can be done by fixing the temperature at two distinct locations, x_j and x_k, for determining $\dot{m}$ and Y_F respectively:

$$T(x_j) = T_{c1}, \tag{8}$$

$$T(x_k) = T_{c2}, \quad x_k > x_j. \tag{9}$$

The implementation of (8) fixes the flame front at x_j and the implementation of (9) gives an interior boundary condition for determining the initial fuel concentration. Theoretically, arbitrary choices for T_{c1} and T_{c2} are permissible. In numerical simulation, however, the choice of a low temperature for T_{c1} and a high temperature for T_{c2} is computationally efficient. In this study, T_{c1} and T_{c2} take values of 400 and 1000 K, respectively.

The second flame configuration is the axisymmetrical counterflow laminar premixed flame. Twin flames are formed near the stagnation plane of the two opposed mixture flows. The governing equations, boundary conditions and solution procedures have been described in detail in our previous publications (Ju, Guo & Maruta 1997*a*; Ju *et al.* 1997*b*). The burner separation distance is fixed at 10 cm in all the calculations. Low Mach number and stagnation point flow approximations are made. Potential flow boundary conditions are employed. The temperature and pressure of the gas mixtures are 300 K and 1 atm, respectively.

The fuel studied in this work is methane. Since the primary interest of the present study is the combined effects of the Lewis number and radiation heat loss, the oxidizer is made by partly replacing N_2 in air with He while keeping the molar concentration of oxygen constant in order to alter the Lewis number of the mixture over a wide range. Four kinds of oxidizers, air, $0.21O_2+0.68N_2+0.11$He, $0.21O_2+0.58N_2+0.21$He and $0.21O_2+0.33N_2+0.46$He, are considered in the present simulation. The computed Lewis numbers of these mixtures at 300 K are respectively 0.967, 1.2, 1.4 and 1.8 near the lean limit. The Lewis number of 1.8 is equivalent to that of a lean propane/air mixture. For very low Lewis numbers, recent numerical simulations with one-step chemistry (Ju *et al.* 1998) and an H_2/air flame (Guo, Ju & Niioka 1998) showed that the extinction curve is still G-shaped and similar to that of a CH_4/air mixture (Ju *et al.* 1997*b*), although a decrease of the Lewis number results in a lower flammability limit. Therefore, our interest here is to investigate how the extinction phenomena change when the Lewis number is increased from a value slightly below unity to a high value close to that of lean propane/air mixture.

The detailed reaction mechanism used in this study is the C_1 chemistry given by Kee *et al.* (1985) which consists of 58 elementary reactions and 19 species (He, N_2,

O_2, H_2, H_2O, H, HO_2, OH, O, H_2O_2, CH, CH, CH_2, CH_3, CH_4, CHO, CH_2O, CO and CO_2). He and N_2 here are treated as inert. Transport properties of these species are evaluated from the CHEMKIN database. The thermal diffusion of H and H_2 is also taken into account.

The governing equations for the above two flame configurations are solved by the modified damped Newton method in conjunction with an improved arclength continuation technique (Smooke 1982; Giovangigli & Smooke 1987; Ju *et al.* 1997*b*).

3. Planck mean absorption coefficients of CO, CO_2 and H_2O

In many previous studies related to flame radiation, the optically thin assumption has been frequently used as an approximation. In the present study, the maximum optical thickness (Ju *et al.* 1997*b*) is less than 0.05 for counterflow flames. Therefore, it is justifiable to neglect the self-reabsorption of radiation of hot burned gas and to employ the optically thin approximation in the counterflow flame. In addition, in order to obtain a comparable standard limit, the optically thin approximation is also used in the calculation of the planar unstrained flame. By further assuming that the major radiating species are CO_2, H_2O, CO and CH_4, the volumetric rate of radiation heat loss in the energy equation, (2), can be written as

$$\dot{q}_r = -K_p \left(4\sigma T^4 - \int_{4\pi} I \, \mathrm{d}\Omega \right) = -4\sigma K_p (T^4 - T_\infty^4), \tag{10}$$

$$K_p = P_{\mathrm{CO_2}} K_{\mathrm{CO_2}} + P_{\mathrm{H_2O}} K_{\mathrm{H_2O}} + P_{\mathrm{CO}} K_{\mathrm{CO}} + P_{\mathrm{CH_4}} K_{\mathrm{CH_4}}, \tag{11}$$

where σ is the Stefan–Boltzmann constant. K_p denotes the Planck mean absorption coefficient of the mixture and is evaluated by the local temperature. P_i and K_i are respectively the partial pressure and Planck mean absorption coefficient of species *i*. I and Ω are the radiation intensity and solid angle of ray, respectively.

The key issue in performing optically thin calculations is the determination of K_p. Tien (1968) presented a series data for K_i for CO, CO_2, H_2O and CH_4 based on a wide-band model. Many studies today still use Tien's data despite significant progress in the development of narrow-band models in the last two decades. A recent microgravity experiment (Wu, Liu & Ronney 1998) indicated that the predicted diameter of flame balls using Tien's data is higher than that of experiment. This discrepancy suggests that the Planck mean absorption coefficients given by Tien might lead to overpredicted radiation heat loss. Therefore, it is of importance to examine the accuracy of Tien's data using the statistical narrow-band model with the recently updated band parameters.

Various narrow-band models have been tested using a line-by-line calculation for conducting and radiating CO_2/air mixtures (Soufiani, Harfmann & Taine 1985). The most accurate temperature and flux distributions were obtained with the randomly statistical narrow-band model (SNB) using an exponential-tailed-inverse line strength distribution (Malkmus 1967). The narrow-band averaged transmittance for an isothermal and homogeneous path $s' \to s$ is given as

$$\bar{\tau}_\nu(s' \to s) = \exp\left[-\frac{\bar{\beta}_\nu}{\pi} \left(\left(1 + \frac{2\pi f p \mid s' \to s \mid \bar{k}_\nu}{\bar{\beta}_\nu} \right)^{1/2} - 1 \right) \right], \tag{12}$$

where the average line width to spacing ratio is $\bar{\beta}_\nu = 2\pi\bar{\gamma}_\nu/\bar{\delta}_\nu$. The narrow-band parameters $\bar{k}_\nu$, $\bar{\gamma}_\nu$ and $\bar{\delta}_\nu^{-1}$ for CO_2, H_2O and CO in the temperature range of 300–

2900 K are provided by Soufiani & Taine (1997). This new data set is for a 25 cm^{-1} wavenumber resolution in the entire wavenumber range and is used in the present calculation of the Planck mean absorption coefficients.

The one-dimensional wavenumber-averaged radiation transfer equation in an absorbing and emitting medium in the x-direction is written as

$$\mu\frac{\partial \bar{I}_v}{\partial x} = -\overline{k_{av}I_v} + \bar{k}_{av}\bar{I}_{bv}. \tag{13}$$

The boundary spectral radiation intensity $\bar{I}_{wv}$ at the left-hand diffusive wall is

$$\bar{I}_{wv} = \epsilon_{wv}\bar{I}_{bwv} + \frac{(1-\epsilon_{wv})}{\pi}\int_0^1 |\mu'|\bar{I}'_v \mathrm{d}\mu', \quad \mu' < 0,$$

where μ is the direction cosine. $\bar{I}_v$ and $\bar{I}_{bv}$ respectively denote the averaged spectral radiation intensity and spectral blackbody radiation intensity over a band width Δv, and $\bar{k}_{av}$ and ϵ_{wv} are the average absorption coefficient and the wall emissivity. The superscript $'$ and subscript w represent the incoming direction and quantities at the wall. Following Kim, Menart & Lee (1990), the narrow-band averaged transfer equation at s along direction Ω is written as

$$\frac{\partial \bar{I}_v(s,\Omega)}{\partial s} = \left(\frac{\partial \overline{\tau_v(s'\to s)}}{\partial s'}\right)_{s'\to s}\bar{I}_{bv}(s) + \bar{I}_{wv}(s_w,\Omega)\frac{\partial}{\partial s}[\bar{\tau}_v(s_w\to s)] + \int_{s_w}^{s}\frac{\partial}{\partial s}\left(\frac{\partial \overline{\tau_v(s'\to s)}}{\partial s'}\right)\bar{I}_{bv}(s')\,\mathrm{d}s' \tag{14}$$

The discretized form of the above equation along a line of sight can be immediately given as

$$\bar{I}_{v,n,i+1} = \bar{I}_{v,n,i} + (1-\bar{\tau}_{v,n,i\to i+1})\bar{I}_{bv,i+1/2} + \overline{C}_{v,n,i+1/2}, \tag{15}$$

where

$$\overline{C}_{v,n,i+1/2} = \bar{I}_{wv,n,1}(\bar{\tau}_{v,n,1\to i+1} - \bar{\tau}_{v,n,1\to i}) + \sum_{k=1}^{i-1}\left[(\bar{\tau}_{v,n,k+1\to i+1} - \bar{\tau}_{v,n,k+1\to i}) - (\bar{\tau}_{v,n,k\to i+1} - \bar{\tau}_{v,n,k\to i})\right]\bar{I}_{bv,k+1/2} \tag{16}$$

and i and n are the spatial and directional discretization index, respectively.

The spectral radiation intensities in an isothermal medium of either pure H_2O, CO_2 or CO at 1 atm between two infinite parallel plates are calculated using the discrete-ordinate method (DOM) (Fiveland 1984; Liu *et al.* 1998). The gas temperature increases from 300 to 2900 K while the wall temperatures are held at 0 K. The wall emissivity is unity. The separation distance between the two plates decreases from 1 to 10^{-5} m to approach the optically thin limit. The S_6 quadrature scheme and 21 grid points were used in the calculations. The total net radiative flux is obtained by integrating the spectral radiation intensity over the whole range of wavenumber and solid angle

$$q(x_i) = \int_0^\infty\int_{-1}^{1}\mu\bar{I}_{v,n,i}\,\mathrm{d}\mu\,\mathrm{d}v = \sum_{\text{all }\Delta v}\left(\sum_{n=1}^{N}\mu\bar{I}_{v,n,i}w_n\right)\Delta v, \tag{17}$$

where N is the total direction number and w_n is the weight function in direction n.

In the optically thin limit, the first term on the right-hand side of (13) can be neglected (assuming the ambient is cold). Therefore, by integrating (13) over all the

Temperature (K)	K_p (H_2O)	K_p (CO)	K_p (CO_2)
300	46.795 78	0.085 34	26.047 47
400	27.619 53	0.324 02	27.626 88
500	18.518 42	0.586 83	30.536 80
600	13.594 47	4.120 13	34.428 30
700	10.123 92	8.439 39	33.239 86
800	7.934 60	6.977 23	30.976 72
900	6.260 79	5.129 98	26.800 22
1000	5.122 63	4.109 91	23.124 49
1100	4.203 39	3.132 42	19.257 40
1300	2.973 98	1.990 50	13.529 17
1500	2.190 70	1.312 17	9.591 12
1700	1.661 26	0.894 45	6.950 19
1900	1.289 21	0.628 20	5.143 53
2100	1.018 91	0.452 99	3.884 88
2300	0.815 69	0.334 32	2.980 17
2500	0.659 69	0.251 82	2.319 46
2700	0.547 77	0.211 37	1.902 07
2900	0.457 61	0.178 90	1.578 58

TABLE 1. The Planck mean absorption coefficients of H_2O, CO and CO_2 calculated from the statistical narrow-band model, K_p: (atm M)$^{-1}$.

wavenumbers and directions and using (17), we obtain

$$\frac{\mathrm{d}q(x)}{\mathrm{d}x} = \int_{-1}^{1}\int_{0}^{\infty} k_{av}\bar{I}_{bv}\,\mathrm{d}v\,\mathrm{d}\mu = 4\pi I_b K_p = 4K_p\sigma T^4. \tag{18}$$

Once the net heat flux is obtained from (17), the Planck mean absorption coefficient K_p can be calculated from

$$K_p = \frac{\mathrm{d}q(x)}{\mathrm{d}x}\Big/4\sigma T^4. \tag{19}$$

The calculated Planck mean absorption coefficients are summarized in table 1.

To demonstrate the validity of the present results, the distributions of the radiative heat loss term, $\mathrm{d}q/\mathrm{d}x$, in the axial direction obtained respectively using Tien's K_p and the present K_p in a counterflow flame are compared in figure 1. The computational conditions are given in the figure. As an accurate solution, the radiative heat loss term calculated from the SNB model with radiation reabsorption is also plotted in figure 1. It can be seen that on the burned gas side, the radiation heat loss term predicted using Tien's data can be about 30 % higher than that of the SNB model. Compared to the results obtained using Tien's K_p (hereafter referred to as Tien's model for convenience), the results based on the present K_p (hereafter referred to as the present model) are much closer to those of the SNB model. The discrepancy between the present model and the SNB model is due to the neglect of the radiation reabsorption in the optically thin model. As can be seen in figure 1, a small region of negative radiative heat loss term (representing energy gain rather than loss) occurs ahead of the flame front ($x = 0.3$) as a result of radiation reabsorption. Therefore, the conclusion can be drawn that Tien's model overpredicts radiation loss of the burned gas by about 30 %. Moreover, the optically thin model overpredicts radiation heat loss through neglecting radiation reabsorption. This conclusion is in agreement also with the results of the microgravity experiment (Wu *et al.* 1998) and the numerical

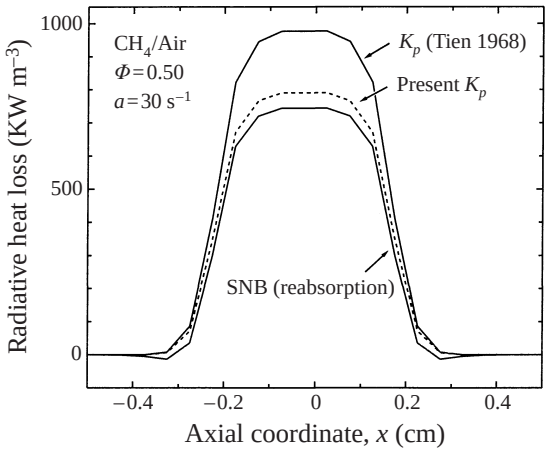

FIGURE 1. Comparisons of the radiative heat fluxes of counterflow flames predicted respectively by the accurate statistical narrow-band model, Tien's model and the present model.

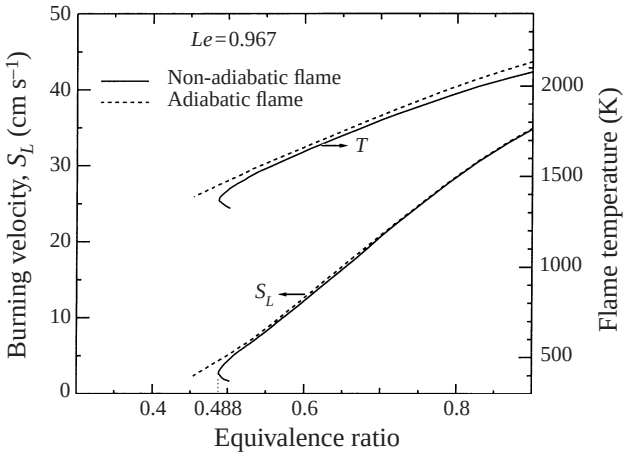

FIGURE 2. Dependencies of flame temperature and burning velocity for adiabatic and non-adiabatic CH_4/air flames.

calculation by Bedir, Tien & Lee (1997) in which different radiation models were compared using the one-dimensional diffusion flame.

4. Standard limits of planar unstrained flames

The laminar burning velocities and the flame temperatures (maximum temperature) of unstrained methane/air flames with and without radiation heat loss are plotted in figure 2 as a function of the equivalence ratio. There are two solutions for each equivalence ratio. The upper is the fast solution and the lower the slow solution. It can be seen that the flame temperature and burning velocity (fast solution) of both adiabatic and non-adiabatic flames decrease dramatically with decreasing the equivalence ratio. Although flame radiation has a considerable effect on flame temperature for equivalence ratios higher than 0.55, its impact on the burning velocity is insignificant. For equivalence ratios lower than 0.55, however, flame radiation causes a dramatic decrease of both the flame temperature and the burning velocity. A turning point showing the

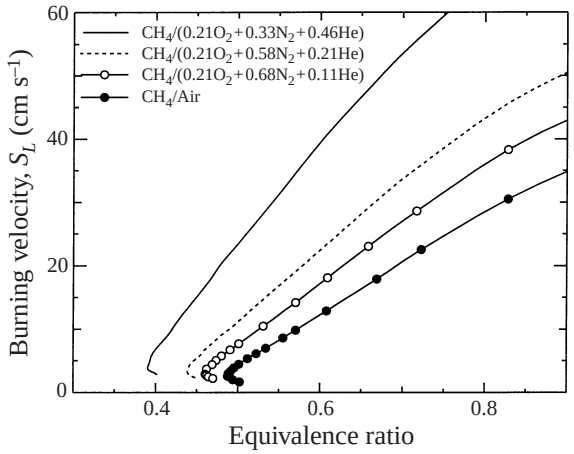

FIGURE 3. Comparisons of burning velocities and flammability limits of CH_4/O_2-N_2-He planar unstrained flames.

flammability limit appears at $\Phi = 0.488$ and $S_L = 2.58$. These limit parameters are close to those predicted by Law (1988) ($\Phi = 0.493$, $S_L = 2.3\,\mathrm{cm\,s^{-1}}$), but slightly different from the experimental data ($\Phi = 0.51$, $S_L = 1.7\,\mathrm{cm\,s^{-1}}$) reported by Ronney (1988). The reason of this discrepancy between simulation and experiment may be largely due to the uncertainty of the chemistry near the lean limit. The corresponding burning velocity of the adiabatic flame at $\Phi = 0.488$ is $4.31\,\mathrm{cm\,s^{-1}}$. The ratio of the burning velocity of the radiating flame to that of the adiabatic flame at the limit is 0.598, which is very close to the theoretical result ($S_L/S_{Lad} = \mathrm{e}^{-1/2}$) given by Buckmaster (1976).

The burning velocities for CH_4/O_2-N_2-He flames with radiation heat loss are shown in figure 3. It can be seen that the flammability limit is extended by partly replacing N_2 in air with He. Since the thermal capacity of He is less than that of N_2, replacement of N_2 with He results in a decrease of the total heat capacity of the mixture. Therefore, for the same fuel and oxygen concentrations, an increase of He concentration causes an increase of the flame temperature and extends the flammability limit. The predicted flammability limit for $CH_4/(0.21O_2{+}0.68N_2{+}0.11He)$, $CH_4/(0.21O_2{+}0.58N_2{+}0.21He)$ and $CH_4/(0.21O_2{+}0.33N_2{+}0.46He)$ mixtures are respectively $\Phi = 0.46$, 0.438 and 0.393. It is interesting to notice that the burning velocity at the extinction limit increases with the increase of He concentration, although the fuel concentration decreases. This is because the high mass and thermal diffusivities of He enlarge the thermal and diffusion thicknesses upstream of the flame front and lead to an increase of radiation heat loss. As a result, a larger radiation heat loss quenches a flame at larger burning velocity.

The calculated limits for unstrained CH_4/O_2-N_2-He flames are the standard limits of the mixtures and will be used to compare with the flammability limits of the corresponding counterflow flames in the following sections.

5. Extinction and bifurcations of counterflow flames

5.1. *The* G*-shaped extinction curve for* CH_4*/air flame* ($Le = 0.967$)

Extinction and flame bifurcation of CH_4/air mixtures have been investigated in our previous study (Ju *et al.* 1997*b*). The results showed a G-shaped extinction curve in the stretch rate–equivalence ratio coordinates (see figure 4). In this study, extinction

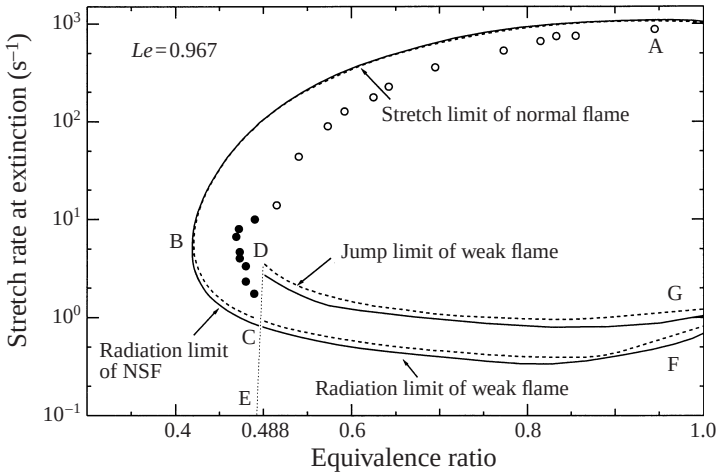

FIGURE 4. Comparison of the G-shaped extinction curves of CH_4/air counterflow flames obtained respectively by the present model (——) Tien's model (- - - -) and by experiment (○, normal gravity experiment by Law *et al.* 1986; •, microgravity experiment by Maruta *et al.* 1996).

of CH_4/air flames is re-examined using the present radiation model. A comparison between the results obtained with the present radiation model and Tien's model is made in figure 4. The experimental data obtained in both normal gravity (Law *et al.* 1986) and microgravity experiments (Maruta *et al.* 1996) are also plotted in figure 4 for comparison.

Curve AB denotes the stretch extinction limit at which the flame is extinguished by stretch-induced incomplete combustion. Branch BC represents the radiation extinction limit at which the flame is quenched by radiation-induced incomplete combustion. Therefore, branches AB and BC respectively represent two distinct extinction limits, the stretch extinction limit and the radiation extinction limit. As indicated by the data points in figure 4, the stretch extinction limit at high equivalence ratios can be observed in normal gravity experiments while the radiation extinction limit can only be observed at a well designed microgravity experiment. In addition, point E in figure 4 denotes the standard flammability limit of the planar unstrained flame obtained in the last section. It can be seen that a mixture leaner than the standard flammability limit can burn when an appropriate amount of stretch is imposed. This phenomenon can be explained by the interaction of the Lewis number effect and radiation heat loss.

We know that the planar unstrained flame at the standard limit is quenched by heat loss through conduction and radiation. We also know that for a mixture with Lewis number less than unity, a moderate stretch can improve the flame while an excessive stretch will quench it (Law 1988; Libby & Williams 1994; Buckmaster 1997). A positive stretch reduces the flame thickness (preheat zone) and the volume of burned gas, and thus suppresses radiation heat loss. Therefore, by imposing an appropriate stretch rate, a mixture below the standard flammability limit can burn in a counterflow configuration. Recent microgravity experiments (Ronney 1985) showed that spherically expanding flames, termed self-extinguishing flames (SEF), can propagate under sub-limit conditions. As the stretch rate decreases, radiation heat loss increases and eventually becomes dominant over enthalpy gain due to the Lewis number effect. The flame then runs into its radiation extinction limit BC. On the

other hand, radiation heat loss decreases as the stretch rate increases. As the flame is pushed onto the stagnation plane, incomplete combustion occurs. When the decrease of radiation heat loss due to flame thinning cannot compensate for the decrease of chemical heat release caused by stretch-induced incomplete combustion, the flame runs into its stretch extinction limit AB. The merging point (B) of the above two curves defines the flammability limit of the counterflow flame. Figure 4 shows that the flammability limit of the counterflow flame (B) is much lower than the standard flammability limit (E). In addition, it is evident that neither the linear extrapolation of the stretch extinction curve AB nor the linear extrapolation of the radiation extinction curve BC to zero stretch rate gives the standard flammability limit.

For equivalence ratios higher than a critical value ($\Phi = 0.5$), the extinction curve opens up and divides into two stable flame branches, a normal flame and a weak flame (see Ju *et al.* 1997*b* for details). The normal flame can be held in the region below curve AB with equivalence ratio higher than 0.5. The weak flame can only be held within the region of curve GDCF. Branches DG and CF are respectively the jump limit and the radiation extinction limit of the weak flame. The jump limit is also caused by the combined effects of the Lewis number and radiation loss reduction. The radiation extinction occurs in the same way as the flames on curve BC. Therefore, within the region GDCF, two kinds of flames exist simultaneously. In addition, a third kind of flame which exists at very low stretch rate and far away from the stagnation plane can be held at a fuel concentration between the standard flammability limit and the opening up limit. Hereafter we abbreviate this far standing weakly stretched flame by FSWSF (a detailed definition will be given in figures 7 and 9). It is interesting that the FSWSF is quenched with an increase of the stretch rate without incomplete combustion even when the Lewis number is lower than unity. Since the flammable region for FSWSF of CH_4/air flames is very narrow, calculation of the whole FSWSF branch is very difficult. A detailed examination of it will be made for CH_4/O_2-N_2-He flames in the following sections. The dotted line DE in figure 4 shows the extinction limit of the FSWSF. Thus it can be seen that only the extrapolation of the extinction limit of the FSWSF to zero stretch rate yields the standard flammability limit (E).

Figure 4 also shows that the calculated extinction results qualitatively agree well with the experimental data, although the predicted flammability limit is lower than the measured limit. The reasons for this discrepancy are manifold. The most important factors which affect the measured limit are burner separation distance and burner diameter. The burner separation distance in the experiment near the flammability limit is 1.5 cm (Maruta *et al.* 1996). However, the preheat zone (1% of temperature rise) predicted in the present study is wider than 3 cm which is much larger than half of the burner separation distance used in the experiment. In addition, at the stretch extinction limit (curve AB), there is only a negligibly small discrepancy between the results of the present radiation model and Tien's model. For the radiation extinction limit (curve BCF) and the jump limit (curve DG), Tien's model gives higher values than the present model. Although it looks like Tien's model predicts results in better agreement with the data than the present model, it does not necessarily mean that Tien's model is more accurate since additional heat loss other than the inherent radiation mechanism, such as conduction heat loss, was imposed in the experiment. In fact, a more recent experiment using a larger burner diameter (4 cm) reduced the measured limit from $\Phi = 0.47$ to 0.45 (Honda 1998).

Another question yet to be answered is how well the employed reaction mechanism works near the flammability limit. Figure 5 shows the effect of chemical kinetics on the flammability limit and the G-shaped extinction curve. It can be seen that

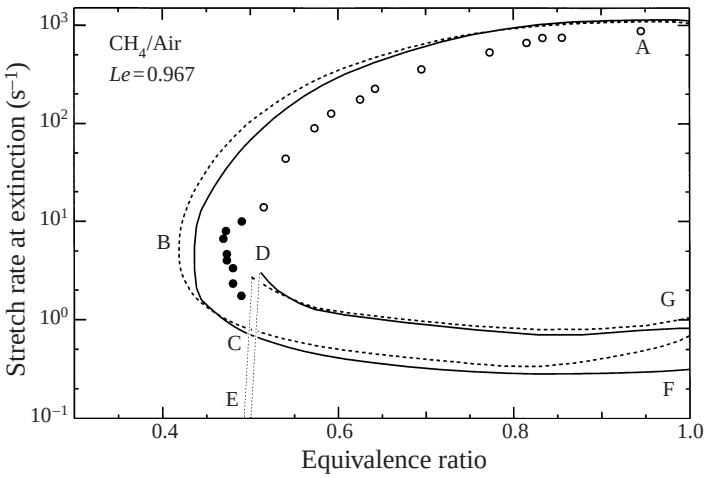

FIGURE 5. Effect of the chemistry on the flammability limit and the G-shaped extinction curves: C_1 (----) and GRI1.2 (——).

chemical kinetics has a considerable effect on the limit of lean flames and the GRI1.2 (Frenklach *et al.* 1995) shows a better agreement with the experiment than the C_1 chemistry. However, the calculated limit parameters ($\Phi = 0.5$ and $S_L = 2.46\,\mathrm{cm\,s^{-1}}$) still have a large discrepancy with the experimental data (Ronney 1988) and the use of GRI1.2 requires a dramatic increase of the computation time. Therefore, to obtain a better comparison between simulation and experiment, it is necessary to investigate the validity of the current reaction mechanism near the flammability limit and to conduct extinction experiments using improved methods in the future.

5.2. *Extinction curve of* $CH_4/(0.21O_2 + 0.68N_2 + 0.11He)$ *flame* ($Le = 1.2$)

In this section, we consider counterflow $CH_4/(0.21O_2 + 0.68N_2 + 0.11He)$ flames. The Lewis number of these mixtures near the flammability limit is 1.2 and the standard flammability limit is $\Phi = 0.46$.

Variations of the flame temperature with the stretch rate for typical fuel concentrations (Ω is the fuel percentage in the mixture) are shown in figure 6. It can be seen that for fuel concentrations below the standard limit, the curve of flame temperature versus the stretch rate is O-shaped and has two limits at a low and high stretch rate respectively. For example, for $\Omega = 4.6$ the stretch rate of 30 s^{-1} is the stretch extinction limit and the stretch rate of 1.6 s^{-1} denotes the radiation extinction limit. These flames occur for mixtures leaner than the standard limit and are located very close to the stagnation plane (see figure 7). Hereafter, we call these flames, which can only exist near the stagnation plane and are bounded by a radiation extinction limit at low stretch and a stretch extinction limit at high stretch, the near stagnation plane flames (NSF, see figures 8 and 9). It will be very interesting to know how the present NSF in the counterflow configuration relates to the spherically propagating SEF defined by Ronney (1985, 1988). The SEF can only be observed for Lewis number less than unity while the NSF can exist even for Lewis number greater than unity. The existence of the NSF isola below the standard limit in figure 6 shows that the flammable region of a $CH_4/(0.21O_2 + 0.68N_2 + 0.11He)$ mixture can still be extended beyond its standard limit in the counterflow configuration, even if its Lewis number

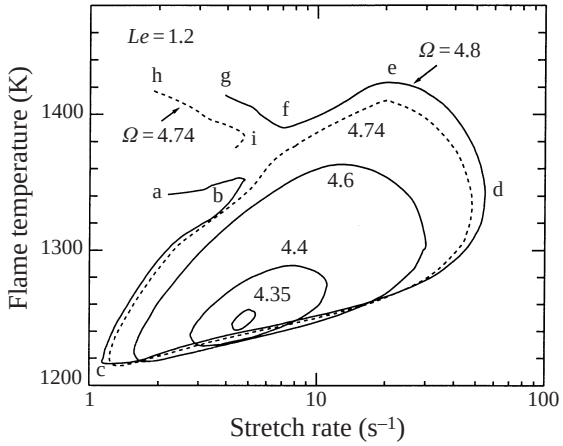

FIGURE 6. Flame temperature profiles plotted as a function of stretch rate for $CH_4/(0.21O_2 + 0.68N_2 + 0.11He)$ flames.

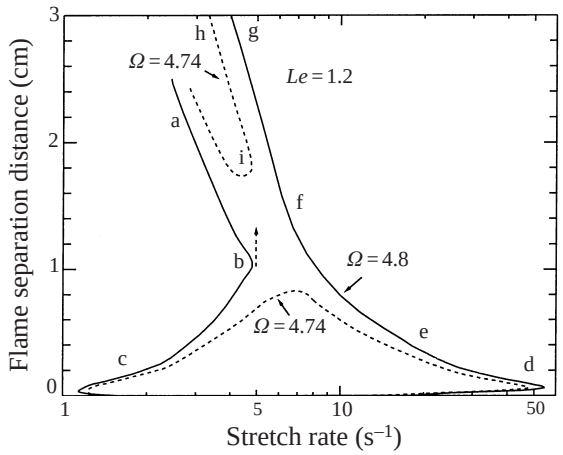

FIGURE 7. Flame separation distances of $CH_4/(0.21O_2 + 0.68N_2 + 0.11He)$ flames at $\Omega = 4.74$ and 4.8.

is higher than unity. It should be emphasized that all the extended flammability limits of the counterflow flames are in fact the limits of the NSF.

The question of why this happens naturally arises and we make an attempt to answer it here. We know that for Lewis number lower than unity, both the Lewis number effect and the reduction of radiation heat loss due to stretch enhance combustion. Therefore, the flammability limit can be extended beyond the standard limit by imposing an appropriate amount of stretch. When the Lewis number is higher than unity, however, the Lewis number effect plays a role counter to that of radiation heat loss reduction. Therefore, an increase of the stretch rate weakens the flame through the Lewis number effect but improves the flame by reducing radiation heat loss. These two factors compete with each other. If the effect of radiation heat loss reduction is stronger than that of enthalpy decrease caused by the Lewis number effect, the flammable region can still be extended, although the Lewis number is greater than unity. This phenomenon becomes more pronounced for a more strongly

radiating mixture since a decrease of the flame thickness reduces radiation heat loss more significantly.

For fuel concentration slightly higher than the standard limit ($\Phi = 4.74$), figure 6 shows that there are two distinct flame branches. The left-hand flame branch is the FSWSF. The FSWSF is a flame above the standard limit and can only exist far from the stagnation plane (see *hi* in figure 7) with a single extinction limit on the large stretch rate side. For the FSWSF branch, flame temperature decreases as the stretch rate increases. At point *i*, the flame is quenched by the Lewis number effect ($Le \geqslant 1$) and the increase of radiation heat loss. It should be noted that the increase of radiation heat loss in this case is caused by the rapid shift of the flame front to the stagnation plane (longer residence time) rather than the decrease of flame thickness. This is understandable by recalling that the FSWSF is quenched by an increase of flame stretch even for $Le \leqslant 1$ (no incomplete combustion). However, the FSWSF does not extinguish as the stretch rate decreases. Unlike the FSWSF, the NSF extinguishes at both high and low stretch rates. Thus, for stretch rates between 1.23 s^{-1} and 2.95 s^{-1}, the FSWSF and the NSF can exist simultaneously with the flame temperature of the FSWSF much higher than that of the NSF.

As the fuel concentration further increases, the strength of the FSWSF becomes greater and its extinction limit moves to the higher stretch rate side. At the same time, the NSF is also strengthened and can be held at a lower stretch rate. The two branches merge with each other at $\Omega = 4.8$. This combination makes the NSF branch open into two parts, *fed* and *bc*. The high-temperature part *fed* joins with the FSWSF branch *gf* and forms a continuous flame branch *gfed*. Since at higher fuel concentrations, the flame on this branch can be observed in a normal gravity experiment, hereafter we call it the normal flame. The normal flame is the flame resulting when the NSF and FSWSF branches merge with each other. The other branch *bc* with much lower flame temperatures can only be observed in a well designed microgravity experiment. Hereafter we call this flame whose temperature is lower than the normal flame the weak flame. As shown in figure 6, the normal flame only has a stretch extinction limit (point *d*) and does not extinguish as the stretch rate goes down. However, the weak flame has a radiation limit at low stretch rate (point *c*) and has a jump limit at point *b*. As the flame approaches point *b*, the reduction of radiation heat loss makes the flame strong enough to move outward (away from the stagnation plane) rapidly. A further increase of the stretch rate will cause the flame jump to the normal flame branch. Examinations for even higher fuel concentrations show that the co-existence of the normal flame and the weak flame is a common phenomenon for equivalence ratios between 0.48 and 1.0.

The corresponding flame separation distances for $\Omega = 4.74$ and 4.8 as a function of the stretch rate are shown in figure 7. It can be clearly seen that for $\Omega = 4.74$, the NSF exists very close to the stagnation flame. A maximum flame separation occurs near a stretch rate around 7 s^{-1}. At a stretch rate larger or lower than 7 s^{-1}, either an increase of stretch or an increase of radiation loss pushes the flame back to the stagnation plane. On the other hand, the FSWSF exists far from the stagnation plane. An increase of the stretch rate makes the FSWSF move quickly towards the stagnation plane. For $\Omega = 4.8$, the normal flame (*gfed*) moves rapidly outward as the stretch rate decreases while extinguishing near the stagnation plane as the stretch rate increases. In contrast, the weak flame (*bc*) is quenched at a low stretch rate at point *c* but moves outward quickly as the stretch rate increases. Finally, at point *b*, a further increase of the stretch rate will make the flame jump from the weak flame branch to the normal flame branch.

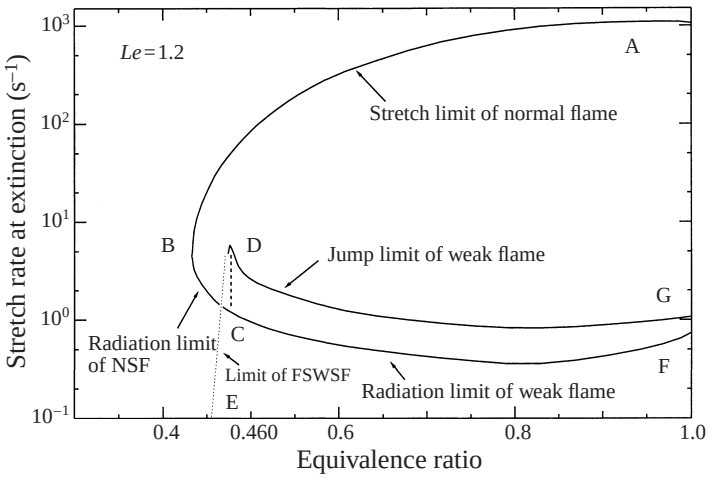

FIGURE 8. The G-shaped extinction curve for $CH_4/(0.21O_2+0.68N_2+0.11He)$ flames.

An extinction curve showing the limits of the FSWSF, the NSF, the normal flame and the weak flames is shown in figure 8. Branch AB denotes the stretch extinction limit of the normal flame and the NSF. Curve BC is the radiation extinction limit of the NSF. The dashed line DE is the extinction limit of the FSWSF. DG and CF respectively represent the jump limit and the radiation extinction limit of weak flames. Figure 8 indicates that there are two kinds of flammability limit, the limit of the NSF (point B) and the limit of the FSWSF (point E). The lower of them represents the flammability limit of the counterflow flame. Figure 8 shows that the extinction curve is still G-shaped and the flammability limit of the counterflow flame is represented by the limit of the NSF and is lower than the standard limit (point E). However, the difference between the flammability limit of the counterflow flame and the standard flammability limit becomes smaller than that shown in figure 4. Moreover, the flammable region of the FSWSF widens as the Lewis number increases.

To provide an easier understanding of the results shown in figures 6–8 and to illustrate the relationship between the planar unstrained flame and the counterflow flame, a schematic graph showing a three-dimensional distribution of the flame temperature as functions of the stretch rate and the equivalence ratio is presented in figure 9. It has been shown that the planar unstrained flame has two solutions, a fast solution and a slow solution (see figures 2 and 3). The fast solution is called the stable flame while the slow solution is unstable (Buckmaster 1997). The merging points of these two solutions are the standard flammability limits, the rich and lean limits of the planar unstrained flame (see the O-shaped curve on the (T, Φ) plane in figure 9). For counterflow flames, due to the competition of the Lewis number effect and radiation heat loss, the extended flame isola (NSF) appears near point B. Φ_0' denotes the extended flammability limit of the counterflow flame. The NSF only exists within a range of moderate stretch rate. For equivalence ratio greater than the standard limit Φ_0, the FSWSF appears at very lower stretch rate. The upper and lower solutions of the FSWSF in the zero stretch limit respectively reduce to the fast and slow solutions of the unstrained flame. As the equivalence ratio further increases, the FSWSF isola merges with the NSF isola and the normal flame and the weak flame are then formed. The heavy solid line on the FSWSF and the NSF isolas denotes the extinction and jump limits of these flames. Its projection on the (a, Φ) plane yields the G-shaped

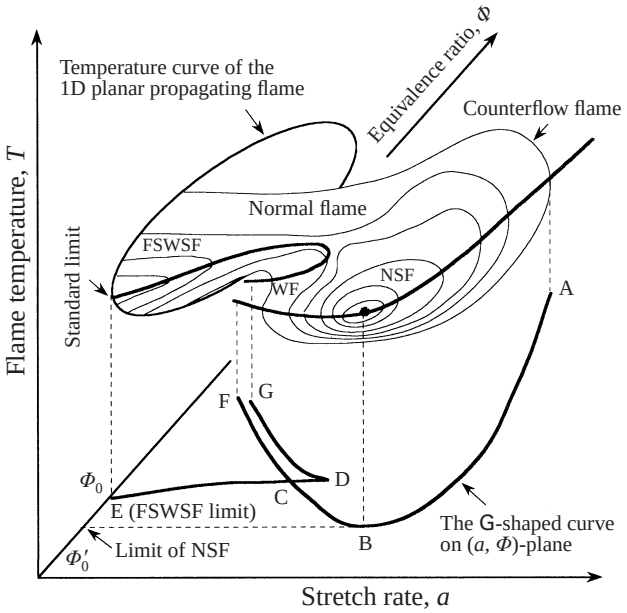

FIGURE 9. Schematic of the relation between the planar unstrained flame and the counter-flow flame.

curve shown in figure 8. Figure 9 shows a clear relationship between counterflow flames and planar unstrained flames. It also indicates that only the extrapolation of the FSWSF extinction limit to zero stretch rate yields the standard limit.

Due to the difficulty of the buoyancy effect and the lack of sufficient theoretical studies on the low-stretched radiative flames, to date the existence of the FSWSF and the branch of the NSF has not been observed in normal gravity experiments. As will be shown below, for most gas mixtures the FSWSF and NSF usually exist at stretch rate below 20 s^{-1}. Therefore, to successfully observe the FSWSF and the NSF branches, microgravity experiments are needed.

5.3. *Extinction curve of* $CH_4/(0.21O_2 + 0.58N_2 + 0.21He)$ *flames at a critical Lewis number* ($Le = 1.4$)

Comparison of figure 9 with figure 4 shows that the difference between the flammability limit of a stretched flame and the standard limit decreases as the Lewis number increases. Therefore, there may exist a critical Lewis number at which the flammability limit of a stretched flame becomes equal to the standard limit. In this section we consider a counterflow $CH_4/(0.21O_2 + 0.58N_2 + 0.21He)$ flame. The Lewis number of a lean mixture is 1.4 and the standard limit of this flame is $\Phi = 0.438$.

Figure 10 shows the flame temperatures as a function of the stretch rate for typical fuel concentrations. It can be seen that the NSF no longer exists for equivalence ratio lower than the standard limit. This is because the impact of enthalpy reduction caused by the Lewis number effect is stronger than the reduction of radiation heat loss due to increased stretch. For fuel concentration slightly higher than the standard limit, the FSWSF and NSF respectively appears at low and high stretch rates. The NSF exists because it is over-stretched but less radiative. Therefore, it has lower flame temperature than the FSWSF. Similar to figure 6, the NSF isola combines with the FSWSF isola as the fuel concentration increases to $\Omega = 4.74$. This combination also

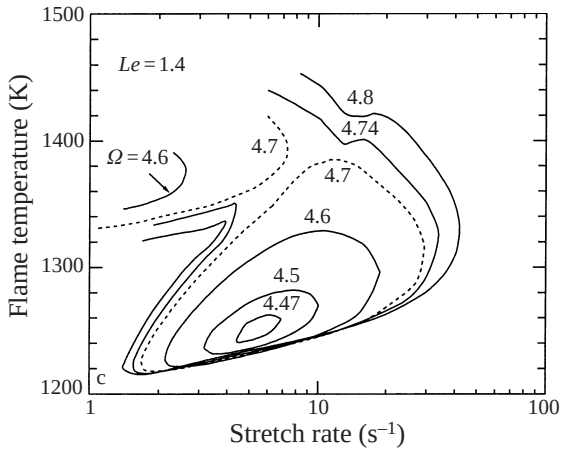

FIGURE 10. Flame temperature profiles plotted as a function of stretch rate for $CH_4/(0.21O_2 + 0.58N_2 + 0.21He)$ flames.

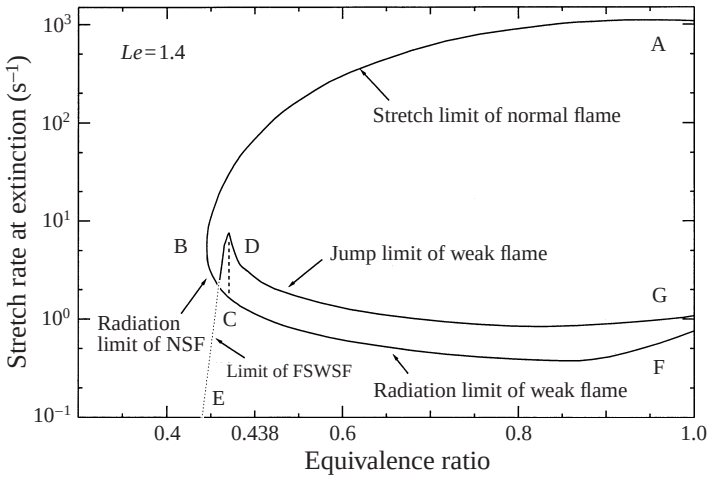

FIGURE 11. The G-shaped extinction curve for $CH_4/(0.21O_2 + 0.58N_2 + 0.21He)$ flames.

produces a normal flame branch and a weak flame branch. Compared to the case of $Le = 1.2$ (figure 6), the FSWSF and the NSF exist at a higher stretch rate. This provides a better condition to observe the FSWSF and NSF in an experiment.

The extinction curve is shown in figure 11. The definition of each curve in figure 11 is the same as that in figure 8. It can be seen that the extinction curve is still G-shaped. However, the flammability limit of the NSF (point B) becomes slightly higher than the flammability limit of the FSWSF (point E). Therefore, the limit of the FSWSF, rather than that of the NSF, now becomes the flammability limit of the counterflow flame. This implies that at high Lewis numbers (higher than a critical value) the flammability limit of the counterflow flame is equal to the standard limit and the flammability limit of the NSF is reduced.

5.4. *Extinction curve of* $CH_4/(0.21O_2 + 0.33N_2 + 0.46He)$ ($Le = 1.8$)

In order to gain insight into phenomena at a Lewis number equivalent to that of a lean propane/air mixture, we here use an oxidizer of $0.21O_2 + 0.33N_2 + 0.46He$. The

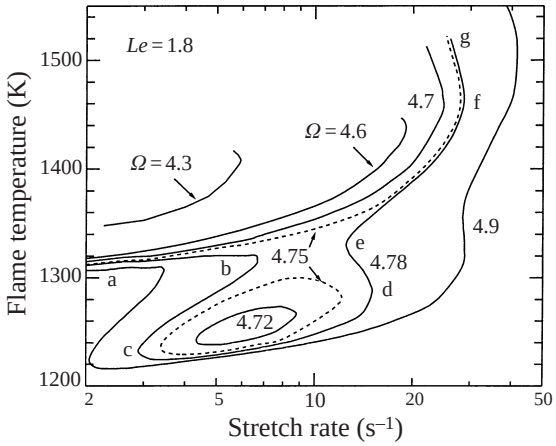

FIGURE 12. Flame temperature profiles plotted as a function of stretch rate for $CH_4/(0.21O_2 + 0.33N_2 + 0.46He)$ flames.

mixture of such an oxidizer with CH_4 has a Lewis number of 1.8, which is almost the same as that of a lean propane/air mixture. The standard limit of this mixture is $\Omega = 3.934$ ($\Phi = 0.39$).

Figure 12 shows the flame temperature as a function of the stretch rate for several typical fuel concentrations. It can be seen that for fuel concentration slightly higher than the standard limit, only the FSWSF exists at the low stretch rate ($\Omega = 4.3$). The NSF does not exist below $\Omega = 4.7$. This is because the Lewis number effect is strong enough to weaken the combustion at high stretch, particularly for low fuel concentrations. As the fuel concentration increases to $\Omega = 4.72$ and further to 4.75, the NSF appears with low flame temperature in a range of moderate stretch rate. This result is different from that obtained by one-step chemistry and constant thermal properties (figure 13). The results of one-step chemistry and constant thermal properties show that the NSF isola and the weak flame on the large stretch rate side does not exist at $Le = 1.8$. This comparison confirms that quantitative predictions require the use of detailed chemistry and transport properties. This is because the competition between radiation heat loss and the Lewis number effect depends strongly on the transport properties in the reaction zone and the preheat zone.

As the fuel concentration further increases to 4.78, the FSWSF isola again merges with the NSF isola (figure 12). Unlike the case of $Le = 1.4$ (figure 10), this combination results in a normal flame (fg) and two weak flames, weak flame I (bc) and weak flame II (de). It should be noted here that the normal flame (fg) at $Le = 1.8$ is just an extension of the FSWSF at high fuel concentration. The two weak flames are the result of the opening up of the NSF branch ($\Omega = 4.75$). As can be seen in figure 12, the normal flame only has a stretch extinction limit at point f. However, the two weak flames have two distinct limits, respectively. Weak flame I (bc) has a radiation limit at point c and a radiation-induced jump limit at point b. On the other hand, weak flame II (de) has a stretch extinction limit at point d and a Lewis-number-effect-induced jump limit at point e. As the fuel concentration further increases, the weak flame I shifts to low stretch rates. However, the weak flame II disappears when fuel concentration is greater than $\Omega = 4.9$. This is reasonable because the NSF is a result of the interaction between the Lewis number effect and radiation heat loss. At high stretch rate, the flame approaches adiabatic conditions. Thus, the weak flame II no

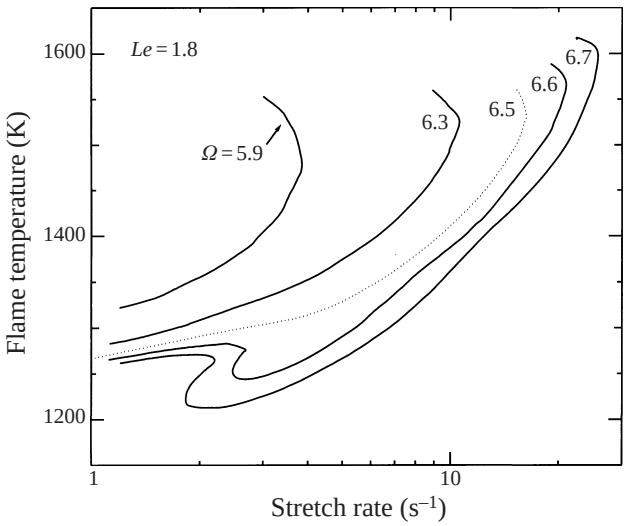

FIGURE 13. Flame temperature profiles plotted as a function of stretch rate with one-step chemistry.

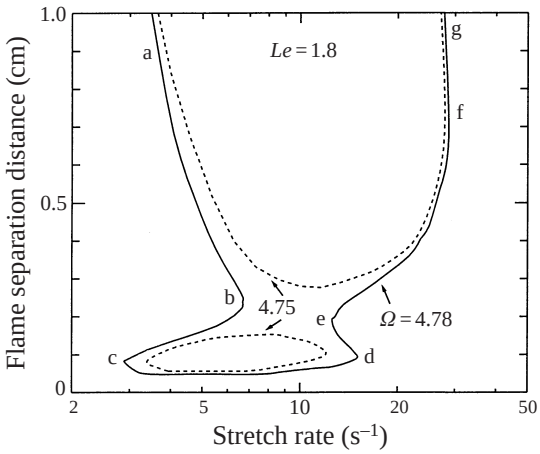

FIGURE 14. Flame separation distances of $CH_4/(0.21O_2 + 0.33N_2 + 0.46He)$ flames at $\Omega = 4.75$ and 4.78.

longer exists when the fuel concentration is high. However, the FSWSF and the weak flame I are different. Both of them exist even for equivalence ratio up to unity.

The flame separation distances for $\Omega = 4.75$ and 4.78 are plotted in figure 14. For $\Omega = 4.75$, the NSF exists very close to the stagnation plane while the FSWSF has a flame separation larger than 0.7 cm (the turning point). Therefore, to observe the near limit FSWSF in experiment, a very large burner separation is required. For $\Omega = 4.78$, figure 14 shows that the flame separation increases rapidly as the weak flames approaches its jump limits *b* and *e*.

The radiation fraction (the ratio of total radiation heat loss to total chemical heat release) for $\Omega = 4.78$ is plotted as a function of the stretch rate in figure 15. It can be seen that at the stretch limit of the normal flame (point *f*) and that of the weak flame (point *d*), the radiation fractions are very low. Thus, the main mechanism for the extinction at these two points is flame stretch. However, at point *c*, the radiation

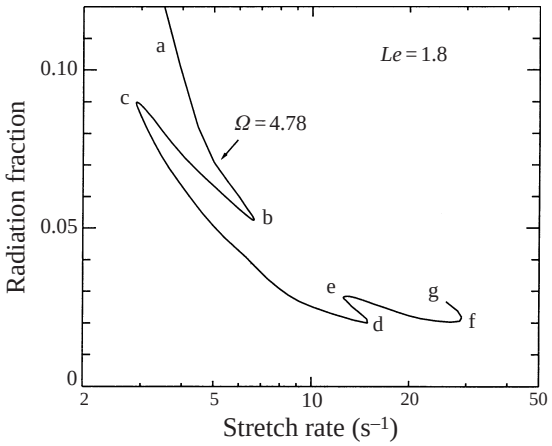

FIGURE 15. Radiation fractions of $CH_4/(0.21O_2 + 0.33N_2 + 0.46He)$ flames at $\Omega = 4.78$ as a function of stretch rate.

fraction is very high. Therefore, flame extinction at point *c* is induced by radiation heat loss. For the same reason, the decrease of radiation fraction around point *b* and the increase of it around point *e* show that the jump limits at these two points are respectively caused by the reduction of radiation heat loss and the weakening of the Lewis number effect.

The extinction curve for $Le = 1.8$ is shown in figure 16(*a*). It can be seen that the extinction curve is no longer G-shaped but instead K-shaped. This transition from a G-shaped curve to a K-shaped curve at high Lewis number agrees with the conclusion of the study using the one-step chemistry (Ju *et al.* 1998), although there are some quantitative differences between them. In figure 16(*a*), AB denotes the stretch limits of the normal flame and the FSWSF. It should be noted again that the normal flame here is just an extension of the FSWSF at high equivalence ratio. Therefore, only after the transition from the G-shaped curve to the K-shaped curve, does the extrapolation of stretch extinction limit of the normal flame to zero stretch rate give the standard limit. HI and IC respectively denote the stretch limit and the radiation limit of the NSF. Therefore, I is the reduced inferior limit of the NSF. Again, the inferior limit is higher than the standard flammability limit. HD and JD represent the stretch extinction limit and the jump extinction limit of weak flame II in figure 12. Thus, D indicates the limit where this weak flame disappears and J is the point where the NSF branch opens up. JG and CF denote the jump limit and the radiation limit of weak flame I in figure 12. This weak flame exists for fuel concentrations above the inferior limit. Therefore, the region below curve ABE is the flammable region of the normal flame and the FSWSF. The region within curve GJDHICF is the flammable region of the NSF and the two kinds of weak flames.

An amplified plot of figure 16(*a*) near the flammability limit is given in figure 16(*b*). It can be seen that although the stretch extinction curve of AB can be extrapolated to the standard limit (E, $\Phi = 0.39$), the extrapolation is not linear. The recent experimental data (Maruta *et al.* 1998) with the same mixture condition are also shown in figure 16(*b*). It can be seen that the measured limits can be separated into two groups, top right group and middle right group. The top right data group is considered to be the stretch limit (AB) and the middle right data are expected to be the bifurcation limits of curve DHIC. If this speculation is correct, these will be the

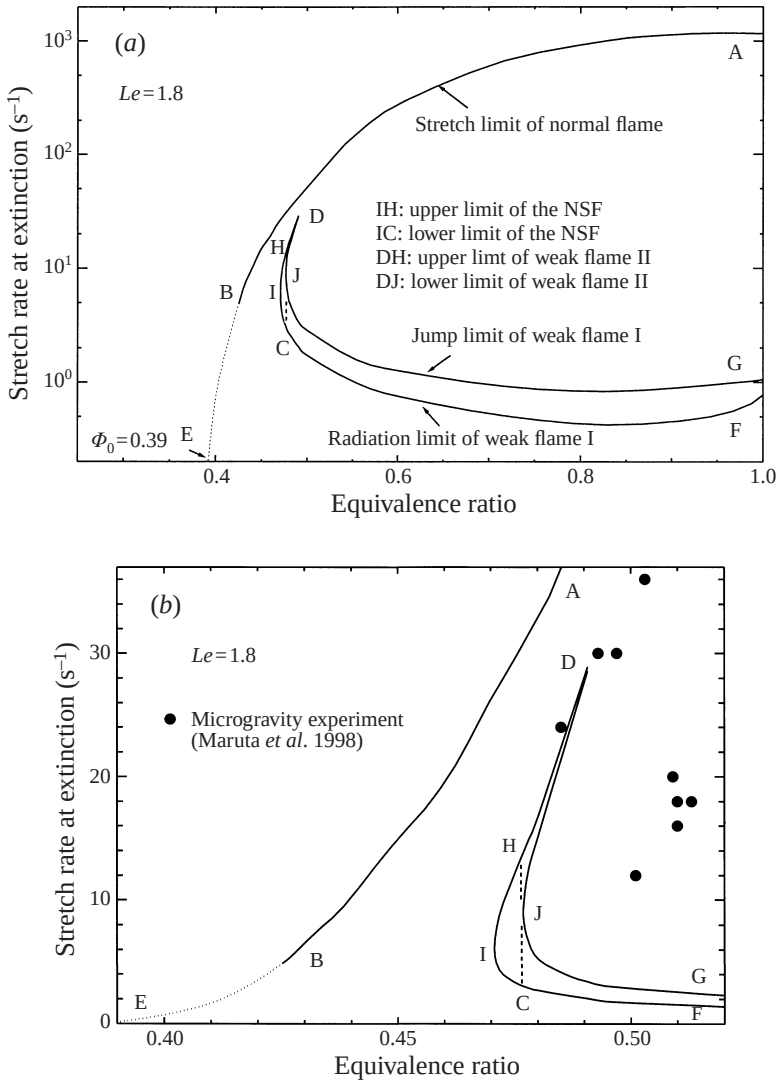

FIGURE 16. Extinction curve for $CH_4/(0.21O_2 + 0.33N_2 + 0.46He)$ flame ($Le = 1.8$), (*a*) a total view, (*b*) an amplified view near the flammability limit and comparison with experiment.

first experiment data to confirm the predicted bifurcations. However, we do not yet have enough experiment data to draw a strong conclusion.

6. Typical flame bifurcations of radiating counterflow flames

Various flame bifurcations have been shown in previous sections. It is useful to summarize how many kinds of flame bifurcation exist in the counterflow configuration and under what conditions they can be observed experimentally.

Eight basic patterns of flame bifurcations are identified and listed in figure 17. The horizontal and vertical axes are respectively the stretch rate and flame temperature. Pattern (1) is the NSF with a radiation extinction limit (*a*) and a stretch extinction limit (*b*) at low and high stretch rates, respectively. This flame can be observed at

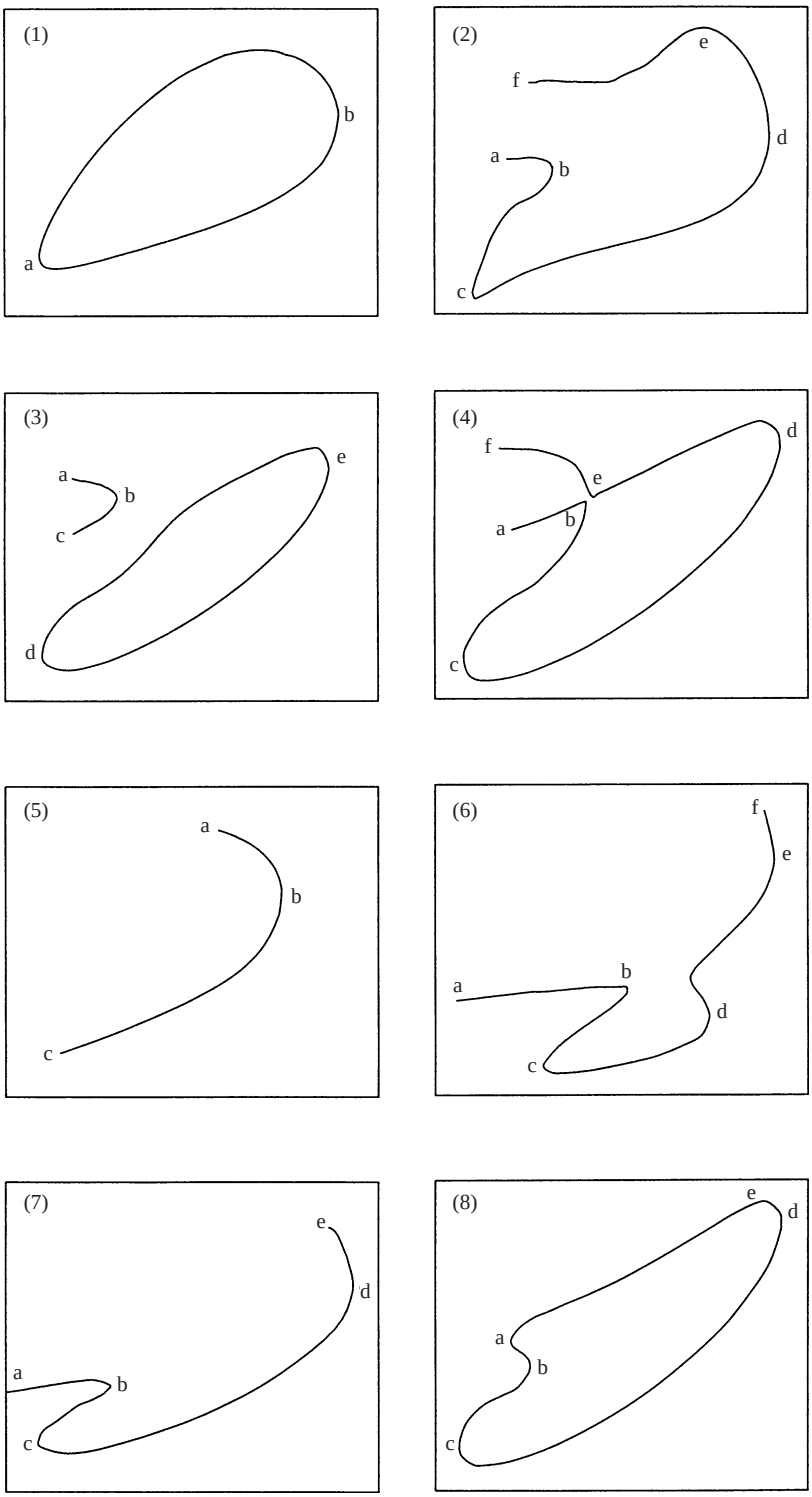

FIGURE 17. Typical kinds of flame bifurcations of the radiative counterflow flames.

an equivalence ratio below the standard limit and for Lewis number less than the critical value Le_{cr}. This critical value is higher than unity and dependent on the radiative characteristic of the mixture. The stronger the flame radiates, the higher this critical value is. In this study, Le_{cr} is about 1.4. This flame can also be observed at equivalence ratio slightly greater than the standard limit when the mixture Lewis number is higher than Le_{cr}.

Pattern (2) is the opening up of the NSF flame shown in pattern (1). This pattern consists of two stable flames, the normal flame *fed* and the weak flame *bc*. This bifurcation occurs for Lewis number slightly less than unity at fuel concentrations higher than the opening up limit ($\Omega = 5.0$ for CH_4/air flame).

Pattern (3) shows that the FSWSF branch *abc* and the NSF branch *de* co-exist simultaneously. This bifurcation occurs for Lewis number equal to or greater than unity at a fuel concentration between the standard flammability limit and the combination limit ($\Omega = 4.74$ in figure 6).

Pattern (4) shows the combination of the FSWSF branch with the NSF branch. Here *fed* is the normal flame and *bc* is the weak flame. This bifurcation occurs for Lewis number between unity and Le_{cr} at a fuel concentration slightly higher than the combination limit. This pattern is a successor to pattern (3) in the above Lewis number range as the fuel concentration increases.

Pattern (5) is the FSWSF branch alone. This pattern occurs at a Lewis number greater than Le_{cr} at a fuel concentration slightly above the standard limit. In this Lewis number range, pattern (3) is the successor to pattern (5).

Pattern (6) shows a combination of the FSWSF branch with the NSF branch occurring at Lewis number greater than Le_{cr} with a fuel concentration between the combination limit and the limit where the weak flame on the high stretch rate side disappears ($\Omega = 4.9$ in figure 12). This combination results in a normal flame and two weak flames.

Pattern (7) is a typical bifurcation for Lewis number above unity at high fuel concentrations.

Pattern (8) is the flame bifurcation at a very low Lewis number (H_2/air flame) at a fuel concentration higher than the opening up limit of the NSF but below the standard limit. This bifurcation is the result of the opening up of the NSF branch at point *b* and consists of two stable flame branches *aed* and *bc*. Here *a* denotes the extinction limit caused by the weakening of the Lewis number effect. Details of this bifurcation have been discussed in Ju *et al.* (1998) and Guo *et al.* (1998).

Linear sensitivity analyses of thermal-diffusive instability of the planar unstrained flame by Sivashinsky (1977) and Joulin & Clavin (1979) showed that a cellular flame structure will be observed for low Lewis number and pulsating flames appear for high Lewis number near the extinction limit. Accurate determination of the flame stability needs a nonlinear sensitivity analysis. Since the present work is limited to the steady-state solutions, the stability of each solution cannot be assessed. Our future work will concentrate on the study of the instability of these branches.

7. Conclusions

New Planck mean absorption coefficients of CO, CO_2 and H_2O are obtained by performing radiative transfer calculations using the statistical narrow-band model. Comparison between the results from the present radiation model and those from Tien's model in a counterflow flame configuration shows that Tien's model overpre-

dicts radiation heat loss by about 30 %. This discrepancy is greatly reduced by the present radiation model.

The extinction and bifurcation of radiating planar unstrained and counterflow CH_4/O_2-N_2-He flames have been investigated numerically using detailed chemistry and the newly developed radiation model. The results showed that the interaction between the Lewis number effect and radiation heat loss dramatically affects flame extinction and bifurcations. It is shown that there exist four kinds of flame regimes: the near stagnation plane flame (NSF), the far standing weakly stretched flame (FSWSF), the weak flame and the normal flame, for radiating counterflow flames. Examination of flame extinction reveals that there are four distinct limits: stretched extinction limit, radiation extinction limit, radiation-induced jump limit and the Lewis-number-effect-induced jump limit. Eight kinds of typical flame bifurcation are demonstrated. The G- and K-shaped extinction curves showing the flammable regions of all the flame regimes are obtained. The transition condition from the G-shaped curve to the K-shaped curve is identified. The results show that the radiation calculation has a great impact on the radiation extinction limit. Accurate evaluation of the radiation sink term requires the radiation reabsorption to be taken into account.

The results also show that there are two kinds of flammability limits: the limit of the NSF and the limit of FSWSF, in counterflow flames. The limit of the NSF can be lower or higher than the standard limit but the limit of the FSWSF is always equal to the standard limit. There is a critical Lewis number at which the two limits become equal. For Lewis number less than this critical value, the limit of the NSF is less than the limit of the FSWSF and the flammability limit of the counterflow flame can be extended by imposing a moderate amount of stretch. For Lewis number larger than this critical value, the limit of the NSF becomes greater than the limit of the FSWSF. Thus, the flammability limit of a counterflow flame is equal to the standard limit and the limit of the NSF reduces to a lower flammability limit. It can be concluded that the extended flammable region is the region of the NSF. Moreover, only the extrapolation of the limit of the FSWSF to zero stretch rate gives the standard limit.

The value of the critical Lewis number is determined by the competition between radiation heat loss and the Lewis number effect. A stronger radiating flame may have a higher critical Lewis number. The results showed that the G-shaped extinction curve evolves into a K-shaped curve when the Lewis number is above this critical value. The experiment-based extrapolation method is valid only if the extinction curve is a K-shaped curve where the normal flame is just an extension of the FSWSF. However, this extrapolation is not linear.

The NSF is a physically intrinsic phenomenon of stretched radiating flames. It may be equivalent to the SEF in the spherically propagating flame configuration. The SEF only exists in a flame with Lewis number lower than unity. However, the NSF can be observed even for Lewis number greater than unity.

The present study reveals a clear relationship between the planar unstrained flame and the counterflow flame. Moreover, it gives a good explanation of the experimental data and provides likely conditions to observe these phenomena in experiment. To achieve an excellent agreement between prediction and experiment, however, requires both the improvement of experimental method and the validation of the chemical kinetics near the flammability limit.

The authors would like to thank Professor Takashi Niioka at the Institute of Fluid Science of Tohoku University for many interesting suggestions and discussions.

REFERENCES

Bedir, H., Tien, J. S. & Lee, H. S. 1997 *Combust. Theory Modelling* **1**, 395–404.

Buckmaster, J. 1976 *Combust. Flame* **26**, 151–162.

Buckmaster, J. 1997 *Combustion Theory and Modelling*, vol. 1, p. 1.

Cetegen, B. M. & Pines, D. S. 1992 *Combust. Flame* **91**, 143–152.

Coward, W. F. & Jones, G. W. 1952 *Bureau of Mines Bull.* 503.

Dixon-Lewis, G. 1994 *Twenty-Fifth Symp.* (*Intl*) *on Combustion*, pp. 1325–1332. The Combustion Institute.

Egolfopoulos, F. N. 1994 *Twenty-Fifth Symp.* (*Intl*) *on Combustion*, pp. 1375–1381. The Combustion Institute.

Fiveland, W. A. 1984 *Trans. ASME*: *J. Heat Transfer* **106**, 699–706.

Frenklach, M. *et al.* 1995 GRI-Mech – an optimized detailed chemical reaction mechanism for methane combustion. *GRI*-95/0058, Nov. 1.

Giovangigli, V. & Smooke, M. D. 1987 *Combust. Sci. Tech.* **53**, 23–49.

Guo, H., Ju, Y., Maruta, K., Niioka, T. & Liu, F. 1997 *Combust. Flame* **109**, 639–646.

Guo, H., Ju, Y. & Niioka, T. 1998 Extinction of counterflow premixed H2/Air flames. *Combust. Sci. Tech.* (submitted).

Honda, A. 1998 A research on low-stretched counterflow flame. Masters thesis, Tohoku University.

Ishizuka, S. & Law, C. K. 1982 *Nineteenth Symp.* (*Intl*) *on Combustion*, p. 327. The Combustion Institute.

Joulin, G. & Clavin, P. 1979 *Combust. Flame* **35**, 139–153.

Ju, Y., Guo, H. & Maruta, K. 1997*a* *Trans. JSME* **63**, 699–704.

Ju, Y., Guo, H., Maruta, K. & Liu, F. 1997*b* *J. Fluid Mech.* **342**, 315–334.

Ju, Y., Guo, H., Maruta, K. & Niioka, T. 1998 *Combust. Flame* **113**, 603–614.

Kee, R. J. *et al.* 1985 *Sandia Rep.* SAND85-8240.

Kim, T. K., Menart, J. A. & Lee, H. S. 1990 *Trans. ASME*: *J. Heat Transfer* **113**, 946–952.

Lakashima, K. N., Paul, P. J. & Mukunda, H. S. 1990 *Twenty-Third Symp.* (*Intl*) *on Combustion*, p. 433. The Combustion Institute.

Law, C. K. 1988 *Twenty-Second Symp.* (*Intl*) *on Combustion*, p. 1381. The Combustion Institute.

Law, C. K. & Egolfopoulos, F. N. 1992 *Twenty-Fourth Symp.* (*Intl*) *on Combustion*, p. 132. The Combustion Institute.

Law, C. K., Zhu, D. L. & Yu, G. 1986 *Twenty-First Symp.* (*Intl*) *on Combustion*, p. 1419. The Combustion Institute.

Libby, P. A. & Williams, F. A. 1994 *Turbulent Reacting Flows.* Academic.

Liu, F., Gülder, Ö. L., Smallwood, G. J. & Ju, Y. 1998 *Intl J. Heat Mass Transfer* **47**, 2227–2236.

Liu, G. E., Ye, Z. Y. & Sohrab, S. H. 1986 *Combust. Flame* **64**, 193–201.

Lovachev, L. A. 1990 *Combust. Sci. Technol.* **20**, 209–216.

Lozinski, D., Buckmaster, J. & Ronney, P. 1994 *Combust. Flame* **97**, 301–316.

Malkmus, W. 1967 *J. Opt. Soc. Am.* **57**, 323–329.

Maruta, K., Yoshida, M., Kobayashi, H. & Niioka, T. 1995 *Proc. 34th Japanese Symp. on Combustion*, p. 414.

Maruta, K., Yoshida, M., Ju, Y. & Niioka, T. 1996 *Twenty-Sixth Symp.* (*Intl*) *on Combustion*, p. 1283. The Combustion Institute.

Maruta, K., Ju Y., Honda, A. & Niioka, T. 1998 *Twenty-Seventh Symp. (Intl) on Combustion.* The Combustion Institute (to appear).

Platt, J. A. & Tien, J. S. 1990 Chemical and physical processes in combustion. 1990 Fall Technical Meeting, Easten Section of the Combustion Institute.

Ronney, P. D. 1985 *Combust. Flame* **62**, 121.

Ronney, P. D. 1988 *Twenty-Second Symp. (Intl) on Combustion*, p. 1615. The Combustion Institute.

Sato, J. 1982 *Nineteenth Symp.* (*Intl*) *on Combustion*, p. 1541. The Combustion Institute.

Sibulkin, M. & Frendi, A. 1990 *Combust. Flame* **82**, 334–345.

Sivashinsky, G. I. 1976 *Acta Astronautica 3*, 889–909.

Sivashinsky, G. I. 1977 *Combust. Sci. Tech.* **15**, 137–146.

Smooke, M. D. 1982 *J. Comput. Phys.* **48**, 72–105.

Sohrab, S. H. & Law, C. K. 1984 *Intl J. Heat Mass Transfer* **27**, 291–300.

Soufiani, A., Harfmann, J. M. & Taine, J. 1985 *J. Quant. Spectrosc. Radiat. Transfer* **33**, 243–257.
Soufiani, A. & Taine, J. 1997 *Intl J. Heat Mass Transfer* **40**, 987–991.
Spalding, D. B. 1957 *Proc. R. Soc. Lond.* A **240**, 83–100.
Sung, C. J. & Law, C. K. 1996 *Twenty-Sixth Symp.* (*Intl*) *on Combustion*, p. 865. The Combustion Institute.
Tien, C. L. 1968 *Adv. Heat Transfer* **5**, 253–324.
Tien, J. S. 1986 *Combust. Flame* **65**, 31–34.
Tsuji, H. 1983 *JSME-ASME Joint Thermal Engng Conf.* p. 11.
Wu, M.-S., Liu, J. B. & Ronney, P. D. 1998 *Twenty-Seventh Symp.* (*Intl*) *on Combustion.* The Combustion Institute (to appear).